Eur. Phys. J. D (2023)77:4
https://doi.org/10.1140/epjd/s10053-022-00586-1

THE EUROPEAN PHYSICAL JOURNAL D

Regular Article – Atomic Physics

Computational approaches to examine the vacuum polarization density

C. Gong[1,2,3], Y. J. Li[3,a], T. T. Xi[4], Q. Su[2,b], and R. Grobe[2,c]

[1] Department of Mathematics and Physics, North China Electric Power University, Baoding 071000, China
[2] Intense Laser Physics Theory Unit and Department of Physics, Illinois State University, Normal, IL 61790-4560, USA
[3] State Key Laboratory for GeoMechanics and Deep Underground Engineering, China University of Mining and Technology, Beijing 100083, China
[4] School of Physical Sciences, University of Chinese Academy of Sciences, Beijing 100190, China

Received 13 April 2022 / Accepted 17 December 2022

Abstract. Based on computational quantum field theory and solutions to the Dirac equation, we show how the vacuum's polarization density induced by strong external field can be calculated based on five independent methods. We compare these methods for a spatially reduced dimensional system and show that some approaches rely on energy renormalizations, energy cutoffs or periodic boundaries. We also illustrate the spatial implications of the breakdown of the linear superposition principle for extremely high intensity fields. A main focus of the article is to discuss future challenges for each approach that might motivate new theoretical and computational studies.

1 Introduction

This is a brief progress report and a roadmap devoted to discussing critically the recent theoretical developments to obtain a better understanding of the vacuum polarization process triggered by external electromagnetic fields and to improve on our computational techniques to study these intriguing and partially counterintuitive processes. The non-linear property of the quantum vacuum is certainly one of the major topics in high field QED physics [1–3], to which the special issue in this journal is devoted. While the possibility to use static charges (such as provided by highly charged nuclei) to probe the response of the vacuum has been pioneered already in the mid 1930s by Dirac [4], Heisenberg [5], Serber [6] and Uehling [7], there are numerous new challenges that need to be addressed if the external field is supercritical, non-Coulombic and even varying in time.

Despite a very rich history of vacuum polarization studies mainly in nuclear physics, to the best of our knowledge, most theoretical studies examined steady state scenarios. In fact, computational techniques that can give us some insight into time-dependent polarization processes have been proposed only recently [8, 9]. These new techniques might supplement more traditional approaches in those situations, where the vacuum is distorted by an external electromagnetic field configuration with a complicated space–time structure.

With very bright light sources planned or being developed, many interesting physical processes may be studied. The affected research areas include, but not limited to, basic and high-energy–density plasma physics, materials and laboratory astrophysics, laser plasma-wake field acceleration and related physics, high-field physics and quantum electro-dynamics, high harmonic generation and attosecond science, particle acceleration (electrons, ions, neutrons, and positrons), and nuclear photonics. Within the high-field physics and quantum electro-dynamics sub-research area, in particular, there are many urgent and unexplored conceptual, theoretical and experimental topics and challenges to be tackled [10–12]. This article intends to shed light on several recently proposed computational algorithms to explore fundamental QED processes.

As relevant high-power pulsed laser fields can vary on very short temporal and spatial scales, traditional approaches that have relied on electron pair creation rates derived from space–time homogeneous fields need to be revisited. There are also conceptual and fundamental issues about the electron–positron pair creation process that have been re-examined recently. For example, it was very difficult to study the detailed dynamics of the electrons and positrons inside the high-field pair creation zone and to separate their birth process from their after-acceleration dynamics with full

Guest editors: Francesco Pegoraro, David A. Reis, Gianluca Sarri, Tongpu Yu.

[a] e-mail: lyj@aphy.iphy.ac.cn
[b] e-mail: qcsu@ilstu.edu
[c] e-mail: grobe@ilstu.edu (corresponding author)

Published online: 04 January 2023

space–time resolution. Recent suggestions based on machine-learning approaches [13] have suggested that it might be possible now to distinguish electrons from positrons inside the interaction region. In another work from last year [14], the relationship between the simultaneous occurrence of vacuum polarization charges and real electron–positron pairs for supercritical fields was studied and it was suggested that these can occur rather independently of each other. The classical view of comparing the vacuum process to the usual polarization mechanism of a dielectric optical medium is inappropriate [15, 16]. In contrast to the polarization of dielectrics, the vacuum's polarization process can occur even in those spatial regions, where the electric field vanishes [14]. This suggests that the conceptual picture, where a local electric field is solely responsible for inducing the charges in the vacuum, is therefore potentially misleading. The proposed high-power laser experiments to systematically test the fundamental properties of the QED vacuum will naturally explore also the electron–positron pair creation regime, where actual charges will be measured as its main signature. It is therefore desirable to accompany these explorations with a better theoretical understanding of the precise relationship between those charges that can be associated with the vacuum polarization and those dynamical charges created due to the supercritical pair-creation process.

To open up the discussion about the general conceptual and theoretical challenges, we illustrate these for a concrete model system. In this work, we will focus mainly on the computational methods and discuss their limitations with regard to visualizing the occurrence of polarization charges in the vacuum. In Sect. 2 we review briefly the key ideas behind computational quantum field theory, which is our central approach, and then devote Sect. 3 to a description of the advantages and disadvantages of various approaches. Two of these methods (Sect. 3.1.2 and 3.2.2) have not been discussed in the literature before. In fact, one of them permits us to contribute to the fundamental discussion about the relativistic spatial localizability of particles. We will finish with an illustration of the spatial consequences of the violation of the linear superposition principle, which can be observed for sufficiently strong external fields.

2 The "physical" situation and its theoretical modelling

We assume that initially there are no real particles in the system, i.e., the initial quantum field theoretical state is given by the Dirac vacuum state $|\Phi\ (t=0)\rangle = |\mathrm{vac}\rangle$. We further assume that a negative charge $-\mathrm{q_{ext}}$ is placed at location $x = 0$ such that it can attract (hidden) positive charges. While this process of introducing a charge out of nowhere would violate the total charge conservation law, it is nevertheless central to the general discussions and derivations in the literature of the vacuum polarization process. As in the usual theoretical descriptions of strong field QED the inclusion of truly photonic interactions can be modeled only within the external field approximation, the Dirac theory for the fermionic response requires the representation of this charge $-\ q_{\mathrm{ext}}$ by its associated electrostatic potential, as provided by the (linear) Maxwell equations. In contrast to the fermionic fields of the Dirac theory, the functional forms of the electromagnetic fields in Maxwell equations are very sensitive to the spatial dimension. For example, our point charge with the associated charge density $\rho_{\mathrm{ext}}(x) = -\mathrm{q_{ext}}\ \delta(x)$ corresponds, according to the stationary Maxwell equation $-\partial^2\ V(x)/\partial x^2 = 4\pi\ \mathrm{k_e}\ \rho_{\mathrm{ext}}(x)$, to an external potential $V(x) = 2\pi\ \mathrm{k_e}\ |x|\ \mathrm{q_{ext}}\ (\equiv E_0|x|)$, where we abbreviate Coulomb's constant as $\mathrm{k_e} \equiv 1/(4\pi\varepsilon_0)$, which is related to the vacuum's permittivity ε_0. With e we denote the positive elementary charge of a positron. The corresponding electric field $E(x) = -\partial V(x)/\partial x = -2\pi\ \mathrm{k_e}\ q_{\mathrm{ext}}\ x/|x|$ does not fall off with the distance to the charge, which is consistent with the real 3D electric field of a charged infinitely extended plate. We should mention, that in order to resemble more a spatially decaying 3D Coulomb force, we could have faked the force field also by choosing an alternative potential of the form $V(x) = -q_{\mathrm{ext}}/(1 + x^2)^{1/2}$. This one leads to a true Rydberg series of electronic bound states and has been pioneered by Eberly and collaborators [17, 18] in strong field photo ionization studies. We note that a screening at $x = 0$ has also been done routinely in nuclear physical calculations [19–21] to study hydrogenic bound states beyond the nuclear charge $Z = 137$, where the ground state energy turns imaginary.

As the fermionic dynamics is restricted to a numerical box of finite size L, we can choose the charge $\mathrm{q_{ext}}$ sufficiently small such that the resulting energy eV ($x = L/2$) is less than $2\mathrm{mc}^2$, i.e. $E_0 < 4\mathrm{mc}^2/(\mathrm{eL})$. This restriction permits us to focus solely here on the vacuum polarization process in the absence of the supercritical pair creation process.

The electrostatic potential $V(x)$ can modify the initial state by inducing a (polarization) charge density from the Dirac vacuum. This density can be determined from the quantum field theoretical expectation value of the time-like component of the electric current operator [22, 23], defined in terms of the electron–positron field operator Ψ as $Q(x,\ t) \equiv -\ e\ (\Psi^\dagger\Psi - \Psi\ \Psi^\dagger)/2$. In the Heisenberg and Schrödinger pictures this density can be calculated as $\rho(x,\ t) \equiv \langle\Phi(t=0)|\ Q(x,\ t)\ |\Phi(t=0)\rangle = \langle\Phi(t)|\ Q(x,\ t=0)\ |\Phi(t)\rangle$.

In traditional nuclear physics, the external charge was typically provided by a nucleus whose charge is an integer multiple of the elementary charge Ze. As the Dirac equation contains the potential energy for the elementary charge e, which is proportional to e ($\mathrm{k_e}$ Ze), the field operator $\Psi(x,\ t)$ depends on powers of ($\mathrm{k_e}\ e^2 Z$). If we include the pre-factor e from the definition of the charge density, and introduce the fine structure constant $\alpha\ [= \mathrm{k_e}\ e^2/(\hbar c)]$, we see that $\rho(x,\ t)$ is proportional to e $(\alpha\mathrm{Z})^{\mathrm{n}}$, with n being an odd integer.

In the Appendix A, we review that the charge density $\rho(x, t)$ can be obtained within computational quantum field theory [24] from the complete set of all time-evolved single-particle wave function solutions to the time-dependent Dirac equation leading to

$$\rho(x,t) = e\sum_p \left[|\phi_p(d,x,t)|^2 - |\phi_p(u,x,t)|^2\right]/2 \quad (1)$$

where the summation extends over the momentum p of these states. While each sum over the positive [negative] energy states $\sum_p |\Phi_p(u,\ x,\ t)|^2 [\sum_p |\Phi_p(d,\ x,\ t)|^2]$ is obviously infinite, the difference of the two sums is finite.

3 Computational procedures, their limitations and open questions

In this section, we will discuss and compare five different numerical approaches to obtain the steady state charge density $\rho\ (x,\ t)$, which characterizes the vacuum polarization. The first two methods (Sect. 3.1) are dynamical and follow the evolution in time starting from $\rho\ (x,\ t = 0) = 0$. The second set of (two) methods (3) uses an energy cut-off in the Dirac-Hilbert space and illustrates how the resulting unavoidable occurrence of unphysical contributions to $\rho\ (x,\ t)$ can be identified and eliminated. The fourth and fifth methods (4) are more traditional and use the energy eigenstates and the lowest-order Feynman diagram. Each of the three subsections is completed with a critical discussion of the advantages and disadvantages of each method including open questions that might motivate further studies.

3.1 Dynamical methods

To follow the time evolution from $\rho\ (x,\ t = 0) = 0$ to $\rho\ (x,\ t)$ is in our opinion the most direct and generally applicable approach to study the dynamical development of the vacuum polarization processes. Here the time-dependent Dirac equation is used to evolve the entire set of all negative and positive energy eigenstates [of the unperturbed Hamiltonian with $V(x) = 0$] in time. As is usually done in computational quantum field theory (CQFT) [2, 24], the evolution of the quantum field operator $\Psi(x,\ t)$ can be determined quite accurately on a finite space–time grid, characterized by N_x spatial and N_t temporal points, using the FFT-based split-operator technique [25–28].

In this approach, the application of the unitary time evolution operator on the quantum mechanical wave functions is sequenced into several repeated steps. In each step, the action of the total evolution operator is approximated by the subsequent application of the kinetic part only which is then followed by the application by the action of the interaction potential. The application of the kinetic part can be performed rather accurately in Fourier space, which also avoids any period doubling problem usually associated with any finite-difference approximation to the momentum operator. The application of the action associated with the potential energy can be performed in position space. As the required back and forth transformations between both representations can be performed rather efficiently using fully vectorizable FFT algorithms, this methodology is in our opinion among the most efficient ones for the Dirac equation.

As a result of the discretization, the underlying infinite dimensional single-particle Hilbert space becomes finite with a total of $2N_\mathrm{x}$ (unperturbed) energies $\pm\ e(p_\mathrm{n})$ given by $e(p_\mathrm{n}) = (m^2c^4 + c^2{p_\mathrm{n}}^2)^{1/2}$ with momentum $p_\mathrm{n} = n\ 2\pi/\mathrm{L}$ and $n = -\ N/2 + 1, -\ N/2 + 2, \ldots, N/2$. The length parameter L is the extension of the numerical box. The characteristic spatial scale of quantum field theoretical dynamics is naturally provided by the fermions' Compton wavelength $\lambda \equiv \hbar/(\mathrm{mc}) = 3.8 \times 10^{-13}$ m, while a typical temporal scale is given by $\tau \equiv \hbar/(\mathrm{mc}^2) = 1.3 \times 10^{-21}$ s, such that $\lambda/\tau = c$ is the speed of light, which is $c = 137.036$ in atomic units.

3.1.1 Adiabatic turn-on of the external charge

There are two extreme limits of turning on the external charge $\mathrm{q_{ext}}$ and therefore the associated potential $V(x)$. In the first case of a very slow turn-on, $V(x)\ f(t)$ is increased to its maximum value $f(t) = 1$ over a sufficiently long time such that the lowest energetic quantum field state, i.e. the bare vacuum state $|\mathrm{vac}\rangle$, evolves adiabatically into the corresponding fully dressed state, denoted by $|\mathrm{VAC}\rangle$. The latter is the lowest energy eigenstate of fully coupled quantum field theoretical Hamiltonian (including the potential V), which can be calculated in terms of bilinear products of the creation and annihilation operators as $H \equiv \int \mathrm{d}x\ \Psi^\dagger(x,\ t = 0)\ h\ \Psi(x,\ t = 0)$.

As we show in Fig. 1, in this case, there are no extra charges created that would escape to infinity.

For very early times, when external charge $\mathrm{q_{ext}}$ is very small, the density develops from $\rho\ (x,\ t = 0) = 0$ to a very narrow distribution around $x = 0$. As $\mathrm{q_{ext}}$ increases, the density's width and height increases, however, keeping the overall shape approximately the same. In other words, even though this is a time-dependent simulation, the density $\rho\ (x,\ t)$ matches at each time the steady state density associated with the instantaneous value of $\mathrm{q_{ext}}$ at that time, as one can expect for a truly adiabatic dynamics.

At first, the accumulation of the positive charge density from zero to its final distribution seems to contradict the required conservation law of the total polarization charge, i.e. $\int_{-L/2}^{L/2} \mathrm{d}x\ \rho\ (x,\ t)$. However, the numerical implementation based on the FFT-method time-evolution exploits periodic boundaries, such that at the boundaries the slope of the potential $\mathrm{d}V/\mathrm{d}x|_{x\ =\ L/2} = -\ \mathrm{d}V/\mathrm{d}x|_{x\ =\ -\ L/2}$ corresponds effectively to an extra positive charge $\mathrm{q_{ext}}/2$ located at $x = \pm\ L/2$, around which a negative charge density builds

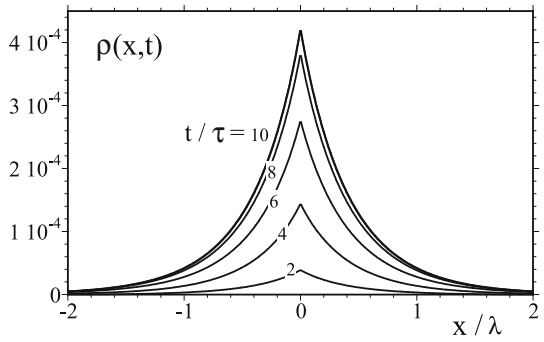

Fig. 1 Adiabatic time evolution of the polarization charge density $\rho(x,\ t)$ as the magnitude of the external charge, centered at $x = 0$ is very slowly increased to its maximal size $q_{\rm ext} = -10$ a.u. via $q_{\rm ext}(t) = -10\ {\rm Sin}^2[\pi t/(2\ T)]$, where long turn-on time is $T = 5.3 \times 10^{-4}$ a.u $(= 10\tau)$. The units of time and space are given by $\tau \equiv \hbar/({\rm mc}^2)$, and $\lambda \equiv \hbar/({\rm mc})$, respectively. [The numerical parameters are: numerical box size $L = 0.146$ a.u. $(= 20\lambda)$ with $N_{\rm x} = 2048$ spatial grid points and spacing $\Delta{\rm x} = 7.1 \times 10^{-5}$ a.u., temporal grid spacing $\Delta{\rm t} = 2.1 \times 10^{-7}$ a.u.]

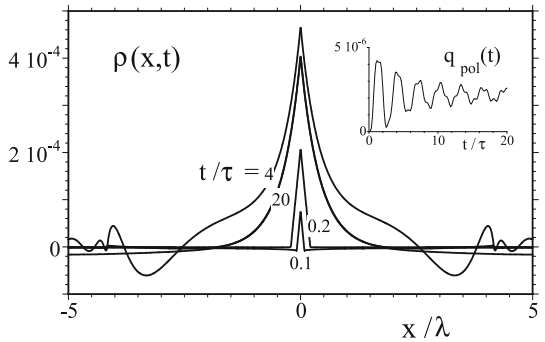

Fig. 2 Time evolution of the charge density $\rho(x,\ t)$ as the result of an abrupt placement of the negative charge $q_{\rm ext} = -10$ a.u. at location $x = 0$. The four snapshots were recorded at four times $t_1 = 5.3 \times 10^{-6}$ a.u., $t_2 = 1.06 \times 10^{-5}$ a.u., $t_3 = 2.1 \times 10^{-4}$ a.u. and $t_4 = 1.06 \times 10^{-3}$ a.u. In the inset we show the growth of the area $q_{\rm pol}(t)$ under $\rho(x,\ t)$ between $x = \pm 0.012$ a.u. $(= \pm 1.64\lambda)$, corresponding to the total amount of the induced charge. [The numerical parameters are: numerical box size $L = 0.367$ a.u. $(= 50\lambda)$ with $N_{\rm x} = 8192$ spatial grid points and spacing $\Delta x = 4.4 \times 10^{-5}$ a.u., temporal grid spacing $\Delta t = 2.2 \times 10.^{-6}$ a.u]

up as well. Therefore, at the boundaries a similar charge accumulation (but with opposite sign) is generated that confirms that the required total charge conservation, i.e., $\int_{-L/2}^{L/2} {\rm d}x\ \rho\ (x,\ t) = 0$ remains indeed valid at all times as one might expect.

3.1.2 Sudden turn-on of the external charge

In contrast to the adiabatic case studied in the prior section, where the time-scales of the temporal growth of any induced charges was entirely dictated by the given time-dependent growth of the external potential V(x) f(t), the case of an abrupt turn-on is from a physical perspective much more interesting as it allows us even to make new observations about the natural time scales of the intrinsic birth process of matter including fascinating new observations concerning the spatial localization properties of polarization charges at birth. As the potential is chosen subcritical, this polarization process should not be confused with the irreversible pair-creation of real electrons and positrons.

While the computations of $\rho\ (x,\ t)$ can presently be performed only in the Heisenberg picture, based on the evolution of the field operator $\Psi(x,\ t)$, the interpretation of the dynamics is easier in the Schrödinger picture, where the quantum field theoretical state $|\Phi(t)\rangle$ is evolved in time. It is advantageous to expand the initial bare vacuum state $|\Phi(t = 0)\rangle = |{\rm vac}\rangle$ in terms of the energy eigenstates of the fully coupled quantum field theoretical Hamiltonian H. This expansion leads to $|{\rm vac}\rangle = c_{\rm VAC}\ |{\rm vac}\rangle + c_\Xi|\Xi\rangle$, showing that the bare vacuum state $|{\rm vac}\rangle$ "contains" already real physical particles as described by the multi-particle state $|\Xi\rangle$, which is orthogonal to$|{\rm vac}\rangle$. Here, the corresponding expansion amplitude $c_{\rm VAC} \equiv \langle{\rm VAC}|{\rm vac}\rangle$ is the overlap between the bare and the physical (fully dressed) vacuum states. The other state $|\Xi\rangle$ is a superposition of various multi-particle states orthogonal to $|{\rm vac}\rangle$. For small external charges $q_{\rm ext}$, the largest contribution to $|\Xi\rangle$ is given by the electron–positron state, followed by a state of two pairs.

In this expansion, the time evolution [after the abrupt turn on of $V(x)$] is given by $|\Phi(t)\rangle = c_{\rm VAC}\ |{\rm vac}\rangle + c_\Xi|\Xi(t)\rangle$, where we assumed that the associated energy eigen value of the vacuum state $|{\rm vac}\rangle$ is zero, such that $c_{\rm VAC}(t) = c_{\rm VAC}$. As a result, the polarization charge density $\rho\ (x,\ t)$ is the sum of a constant and a time-dependent part, $\rho\ (x,\ t) = |c_{\rm VAC}|^2\ \langle{\rm VAC}|\ Q(x,\ t = 0)\ |{\rm VAC}\rangle + \rho_\Xi(x,\ t)$. The second part, which is time-dependent, is given by $\rho_\Xi(x,\ t) = |c_\Xi|^2\langle\Xi(t)|Q(x,\ t = 0)\ |\Xi(t)\rangle + c_{\rm VAC}\ \langle{\rm VAC}|\ {\rm Q(x,t = 0)}\ |\Xi(t)\rangle$ + c.c.

This expansion suggests the following picture for formation of the steady state density $\rho_{\rm pol}(x) \equiv \langle{\rm VAC}|\ Q(x,\ t = 0)\ |{\rm VAC}\rangle$as illustrated in Fig. 2. The formation of the build-up of the positive charge density around $x = 0$ is only qualitatively similar to the one of Fig. 1, however, and in contrast to the adiabatic evolution of Fig. 1, here additional charged particles have been created [and likely associated with $\rho_\Xi(x,\ t)$] that escape away from $x = 0$.

At early times, the observed triangular shape of $\rho\ (x,\ t)$ seems to mirror the spatial structure of the underlying potential $V(x)$ associated with $q_{\rm ext}$. In contrast to the (shape-invariant) adiabatic growth of $\rho\ (x,\ t)$ displayed in Fig. 1, we observe here an entirely different growth pattern as well as a different (triangular-like) shape. In fact, at our two earliest recorded times (t_1 and t_2), the observed length of the triangle's base extends almost precisely from $-\ c\ t_{\rm n}$ to $c\ t_{\rm n}$. This observation clearly suggests that any induced positive charges from the vacuum were exclusively created only at $x = 0$, where the *point* charge $-q_{\rm ext}$ was originally placed at t

= 0, and charges do not occur in its immediate vicinity. This extremely sharp localization is actually quite interesting from a fundamental point of view [29–31]. It certainly supplements many prior studies of pair creation [24], where a (minimum) length scale is typically given by the electron's reduced Compton wavelength λ, which is significantly wider than the extension of the observed induced positive charge cloud in Fig. 2. It is also a challenging to interpret this interesting localization feature with the corresponding Heisenberg-like uncertainty principle suitable for charge densities.

As the induced charge grows, we see that the original triangular shape of $\rho\ (x,\ t)$ changes. The outgoing portion of the charge density becomes even oscillatory, reflecting possibly the interesting time-dependent interference patterns of the outgoing positronic and electronic contributions. For times longer than about t $\approx 20\tau$, we see that close to the point charge a steady state vacuum charge cloud has been established, which no longer changes in time. To better estimate the temporal scale, we have displayed in the inset the growth of the total positive induced vacuum polarization charge density, $q_{\rm pol}(t) \equiv \int {\rm d}x\ \rho\ (x,\ t)$ where we have extended the integration region extend from $x = -0.012$ a.u. to 0.012 a.u.. We see that the actual induced charge approaches its characteristic asymptotic steady state value in a rather oscillatory fashion, which is not unusual in view of the sudden turn-on of the potential $V(x)$. The resulting total charge $q_{\rm pol}(t)$ approaches asymptotically a value of around 2.2×10^{-6} a.u., which is slightly less than the amount 2.7×10^{-6} a.u., obtained from Fig. 1 for $q_{\rm ext} = 10$ a.u.. This is consistent with the fact that $|{\rm c_{VAC}}|^2 = |\langle {\rm VAC}|{\rm vac}\rangle|^2$ is slightly smaller than unity for our parameters.

3.1.3 Points of critique and open questions

In order to obtain the most accurate steady state distribution $\rho_{\rm pol}(x)$ from this time-dependent approach, it would be desirable to maximize the interaction duration to provide sufficient time for all particles to escape from the creation region around $x = 0$. Unfortunately, due to the required spatial periodicity and additional particles returning back to $x = 0$ from the boundaries at $x = \pm\ L/2$, this reversal time cannot be chosen arbitrarily large due to the occurrence of unwanted supercritical pair creation mechanism (see above) for a too large box size L. A recently published article [14] addresses the interesting question, how the virtual charges associated with the vacuum's polarization are related to the real physical particles that are created when the potential is chosen supercritical.

One can certainly understand that the total charge conservation is a global property and that it is guaranteed in our specific numerical situation by the periodic boundaries, where the reversed charges are created. However, we were surprised that charge conservation within larger spatial domains around $x = 0$ is even not guaranteed. In the traditional picture, the vacuum is visualized as a dielectric medium where virtual electron–positron dipole pairs can be rearranged by an external field. However, this particular picture seems to be inconsistent with the observed growth of mainly positive charges at $x = 0$ and the absence of any negative charges of similar magnitude nearby. While one might consider time-dependent techniques as merely indirect theoretical tools to determine the steady state charge distributions, we like to point out that they might also play an important future role in simulating short-time non-stationary process, which is quite relevant for interactions induced by ultra-short laser pulses.

3.2 Energy-cutoff based approaches

While the prior methods require the summation of the entire (in principle infinite) Hilbert space, one could imagine that due to the finite value of the external charge $q_{\rm ext}$ only states with lower and intermediate energies might be required for an accurate determination of the vacuum polarization. At first, it seems, therefore, reasonable in order to decrease the computational time and also the memory requirements, to introduce an effective cut-off energy $E_{\rm cut}$ and exclude all those states from the calculation in Eq. (1), whose magnitude of the energy is larger than a chosen $E_{\rm cut}$. This reduction leading to $\rho_{\rm cut}(x,\ {\rm t})$ might be computationally advantageous especially for calculations in higher than just one spatial dimension. However, as we will show below, any artificial energy cut will introduce some extra spurious contributions to the density $\rho_{\rm cut}(x,\ t)$, denoted by $\rho_{\rm spu}(x,\ t)$, which (due to their additive nature) can be subtracted out by either instantaneous approaches (Sect. 3.1.1) or dynamical methods (Sect. 3.2.2).

3.2.1 Instantaneous removal of the spurious contributions based on the FW theory

In Fig. 3, we have repeated a similar simulation for $\rho(x,\ t)$ as already displayed in Fig. 2, but this time, in the required summation over the time-evolved negative and positive energy states we have omitted contributions of states whose energy has a magnitude of larger than $E_{\rm cut} = 257.36\ {\rm mc}^2$. As a reference, we should mention that for our numerical parameters ($N_{\rm x} = 8192$ and $L = 0.367$ a.u.) the entire Hilbert space is discrete with a largest possible energy given by $514.72\ {\rm mc}^2$. We observe that in this case $\rho_{\rm cut}(x,\ t)$ is characterized by the occurrence of rather triangularly shaped density, denoted by $\rho_{\rm spu}(x,\ t)$, which grows in a shape invariant matter with its base line extending from $x = -\ c\ t$ to $x = c\ t$. The dynamics of these purely mathematical solutions is well understood from a mathematical aspect [8]. In this article from 2014, analytical expressions as well as their relationship to the Maxwell equations were established, but their direct physical interpretation is still not fully understood to date. There are two immediate observations that suggest a purely mathematical character of these particular (numerically fully converged) solutions. The solutions grow without any limit if the numerical box length L is sufficiently long, and the charges which

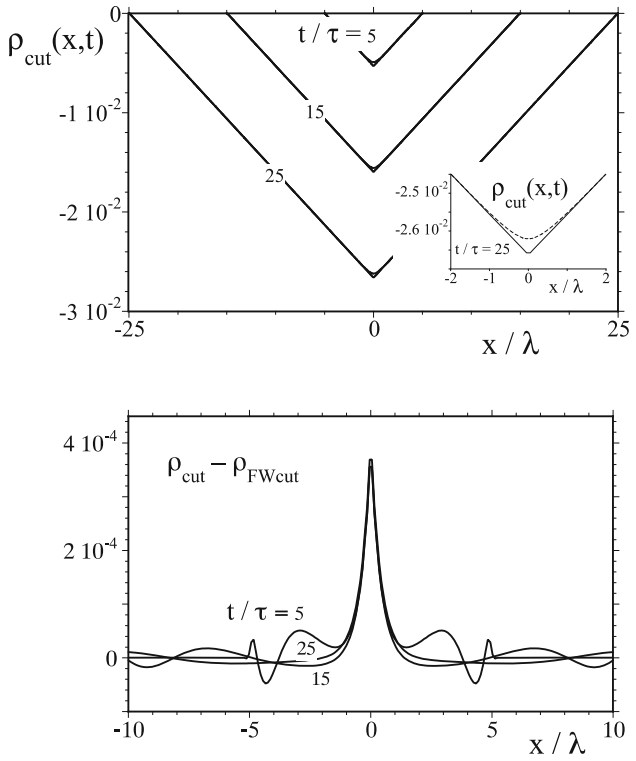

Fig. 3 **a** Snapshots of temporal evolution of the vacuum polarization charge density $\rho_{\rm cut}(x,\ t)$ at times $t_1 = 2.67 \times 10^{-4}$ a.u. $(= 5\tau)$, $t_2 = 8 \times 10^{-4}$ a.u. $(= 15\ \tau)$ and $t_3 = 1.33 \times 10^{-4}$ a.u. $(= 25\tau)$ indicated by the dashed lines. In the calculation of $\rho_{\rm cut}(x,\ t)$ the maximum energy of the Hilbert space was limited to $E_{\rm cut}/({\rm mc}^2) = 257.36$. For comparison, the largest energy of the Hilbert space is associated with $E/({\rm mc}^2) = 514.72$. The corresponding continuous lines are the corresponding densities $\rho_{\rm FWcut}(x,\ t)$ obtained by the Foldy-Wouthuysen theory with the same cut-off energy. **b** The corresponding three physical polarized charge densities obtained by the subtraction by $\rho(x,\ t) \equiv \rho_{\rm cut}(x,\ t) - \rho_{\rm FWcut}(x,\ t)$. The densities match the ones perfectly computed in Fig. 2 for the abrupt turn-on of $-\ q_{\rm ext} = -\ 10$ a.u. [The numerical parameters are: numerical box size $L = 0.367$ a.u. $(= 50/c)$ with $N_{\rm x} = 8192$ spatial grid points and spacing $\Delta x = 4.4 \times 10^{-5}$ a.u., temporal grid spacing $\Delta t = 3.55 \times 10^{-7}$ a.u]

appear to accumulate around the (originally given) negative charge are also negative. While an infinite growth does not necessarily violate any energy conservation [8], the accumulation of like charges around the central charge seems unphysical to us. We also direct the reader to the detailed structure of the tips of each triangle, which appear to be rounded. This is a very important detail as these tips contain the actual physical polarization density $\rho(x,\ t)$ as we show below.

The second set of data (continuous lines) was obtained by the (energy cut off) charge density associated with the corresponding Foldy-Wouthuysen (FW) theory [32] characterized by the Hamiltonian

$$h_{FW} = \sigma_3(m^2c^4 + c^2p^2)^{1/2} + e\,V(x) \qquad (2)$$

As this Hamiltonian $h_{\rm FW}$ is diagonal in spinor space it cannot predict any transitions between the positive and negative energy levels and fails to reproduce those processes that involve the electron–positron pairs such as the polarization. This means that states of the positive (negative) energy manifold have only a non-vanishing upper (lower) spinor component and the corresponding FW charge density, i.e., $\rho_{\rm FW}(x,\ t) = (e/2)\ \sum_{\rm p}\ [|\,W(d,\ p,\ x,\ t)|^2 - |\,W(u,\ p,\ x,\ t)|^2]/2$ is identical to zero at any time, where $W(d,\ p,\ x,\ t = 0)$ and $W(u,\ p,\ x,\ t = 0)$ are the eigenstates of $\sigma_3\ (m^2c^4 + c^2p^2)^{1/2}$. This can be seen most easily as the space spanned by all positive energy states, is already complete with regard to the first spinor component, i.e., $\sum_{\rm pu} |{\rm pu}> <{\rm pu}| = 1$. We therefore have $\sum_{\rm p}\ |\,W(u,\ p,\ x,\ t)|^2 = \sum_{\rm p}\ W(u,\ p,\ x,\ t)\ W(u,\ p,\ x,\ t)^\dagger = \sum_{\rm p}\ \langle x|U(t)|u;\ p\rangle\ \langle u;\ p|U(t)^\dagger|x\rangle = \langle x|x\rangle$. And similarly, we have $\sum_{\rm p}\ |\,W(d,\ p,\ x,\ t)|^2 = \sum_{\rm p}\ \langle x|U(t)|d;\ p\rangle\langle d;\ p|U(t)^\dagger|x\rangle = \langle x|x\rangle$ and therefore $\rho_{\rm FW}(x,\ t) = \langle x|x\rangle - \langle x|x\rangle = 0$ vanishes identically if all states are taken into account. But, nevertheless, this density becomes quite useful when it is calculated for the same energy cut-off as used in the Dirac data. In this case, $\rho_{\rm FWcut}(x,\ t)$ seems to be identical to the spurious contributions $\rho_{\rm spu}(x,t)$.

The data in Fig. 3 suggest this remarkable similarity [9] between $\rho_{\rm FWcut}(x,\ t)$ and $\rho_{\rm cut}(x,\ t)$. In fact, at each time, the only difference can be found at the tip of each triangle, close to $x = 0$, as the Dirac density does contain the physical vacuum polarization density in addition to $\rho_{\rm spu}(x,\ t)$. In contrast to the rounded tips observed for the Dirac theory, the tips obtained from the Foldy-Wouthuysen theory seem more like a real cusp. In the inset of the Figure, we have subtracted the densities from each other, $\rho_{\rm cut}(x,\ t)\ -\ \rho_{\rm FWcut}(x,\ t)$ at each of the three times. For all three moments in time, this difference agrees with the actual physical vacuum polarization density $\rho(x,\ t)$ obtained in Figs. 2 without cut-off. This numerical observation suggests that it is indeed possible to restrict the Hilbert space of possible states and still being able to recover the desired physical charge density via this subtraction scheme.

In order to better understand the dependence of these spurious triangular solutions, we have shown in Fig. 4 the density $\rho_{\rm cut}(x,\ t)$ at time $t = 8 \times 10^{-4}$a.u., but for eight different cut-off energies $E_{\rm cut}/{\rm c}^2 = 3$, 4, 5, 6, 7, 20, 31 and 32. The nice numerical convergence with increasing cut-off energy up to $E_{\rm cut} = 31\ {\rm c}^2$ seems to (falsely) suggest that we have obtained numerically convergent and reliable physical data. However, this conclusion is dangerous and wrong. In fact, the spurious solution seems to be reduced for the even larger cut-off $E_{\rm cut} = 32\ c^2$ and also seems to violate causality as the density extends here beyond the light cone. In fact, for a slightly larger energy 32.19 c^2, the entire spurious contributions have entirely disappeared, reflecting the fact that now the complete Hilbert space has been taken into account. This shows that those states that are close to the largest energy in the finite Hilbert space play an absolute crucially important role with regard to the density $\rho_{\rm cut}(x,\ t)$.

This unexpected finding might not necessarily be in contradiction to prior observations of divergent solutions. In fact, the very highest energetic states in our finite Hilbert space might possibly represent the accumulative effect of all those other states that are energetically outside of our complete set of Hilbert states.

3.2.2 Periodic self-cancellation of the spurious contributions

There is also a second (and independent) method that permits us to remove the spurious contributions to the charge density without relying on the computation of the solutions to the Foldy-Wouthuysen theory. As we have mentioned above (in Sect. 3.1.1), our solutions to the Dirac equations require periodic boundaries, leading to the well-known wrap-around effect that particles entering the right boundary at $x = L/2$ will re-appear at $x = -L/2$. Furthermore, the corresponding extra positive charges $q_{\rm ext}/2$ at $x = \pm L/2$, lead also to the formation of triangularly shaped solutions, but with an opposite sign. We note that the effect of these periodic boundaries on the evolution of the growing triangles for longer times than $L/(2c)$ can be best visualized by extending the box size to infinity and summing up triangles that grow around the locations $x = \pm n\ L$ together with inverted triangles that are centered at $x = \pm (2n + 1)\ L/2$, with $n = 0,1,2,3 \ldots$ If we add up all of these triangularly shaped densities, it turns out that there at specific moments in time, when they will perfectly interfere distractively as they propagate through each other. These means that there are periodically re-occurring moments in time, when we have a perfect overlap and distractive interference around $x = 0$. As a result of these perfect distractive cancellations of all these unphysical contributions, only the physical contributions to the polarization density survive and therefore can be recovered. In other words, at re-occurring times $t_n = n\ L/c$, with $n = 1,2, \ldots,$ the system autocorrects itself and we can obtain the exact charge polarization density, without the need of any other subtraction scheme.

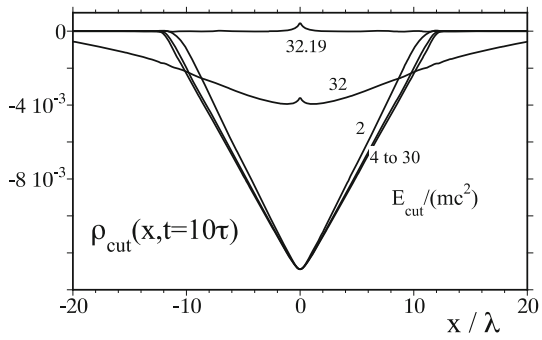

Fig. 4 The vacuum polarization density $\rho_{\rm cut}(x,\ t)$ at time $t = 6.6 \times 10^{-4}$ a.u. $(= 12.5\tau)$, but where the summation has been limited to different amounts for the energy cut-off: 2, $4 < E_{\rm cut}/(\mathrm{mc}^2) < 32$. The top most graph is without any cut-off, associated with the $E/(\mathrm{mc}^2) = 32.19$, which is the largest energy in the Hilbert space for $N_{\rm x} = 1024$ and $L = 0.730$ a.u. $(= 100\lambda)$

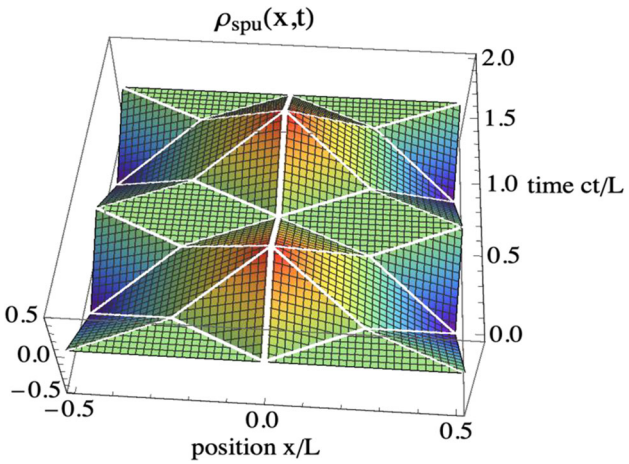

Fig. 5 Sketch of the space–time evolution of the unphysical triangular contributions $\rho_{\rm spu}(x,\ t)$ to the charge density under periodic boundaries at $x = \pm L/2$. The density starts with $\rho_{\rm spu}(x,\ t = 0) = 0$ after a perfect cancellation at times L/c and $2\ L/c$ it returns back to zero everywhere; i.e. $\rho_{\rm spu}(x,\ T) = 0$

3.2.3 Points of critique and open questions

While these spurious contributions do not occur if the complete set of Hilbert states is included in the determination of $\rho(x,\ t)$, one would naturally (but apparently incorrectly) expect that including states with sufficiently large energy (but not all) should -in principle- be sufficient for their removal. However, while the data in Fig. 4 confirm that there is indeed a huge region of states (between energies $E = 3\ \mathrm{mc}^2$ and $31\ \mathrm{mc}^2$) that is dynamically irrelevant (as one would expect), suddenly important contributions show up for states close to the largest energy of the system. This observation is even more puzzling, as we can increase the amount of the upper energy limit of these important edge states by arbitrarily choosing a larger and larger number of spatial grid points $N_{\rm x}$. It seems obvious that the time evolution of these edge states has to be qualitatively different than the one for lower energetic states. Certainly, more systematic studies are required here. The similarity to the states obtained by the FW theory is also interesting, however, as we suggested above, here the edge states do not play any role (Fig. 5).

As any energy cut-off might be required to handle truly infinite Hilbert spaces, associated with the continuum limit $N_{\rm x} \to \infty$ and $\Delta_x \to 0$, it would be beneficial to better understand how the FW theory can provide the correct corrections to remove the spurious solutions. Most importantly, in three-dimensional calculations, these energy-cutoffs can not only significantly reduce the CPU time, but they can make these quantum field theoretical studies possible in the first

place. In 1D, the mathematical structure of the spurious solutions can be modeled very well by a simple wave equation [8], where a term that is proportional to $q_{\rm ext}(z)$ acts as a source term $(\partial_{\rm ct}{}^2 - \partial_{\rm x}{}^2)\ \rho_{\rm spu}(x,\ t) = 8\pi\ \chi\ q_{\rm ext}(x)$, with the (numerically determined) proportionality factor $\chi = 1.15 \times 10^{-3}$ a.u. If we assume the two initial conditions $\rho_{\rm spu}(x,\ t = 0) = \partial_{\rm t}\ \rho_{\rm spu}(x,\ t = 0) = 0$, the inhomogeneous solution reads $\rho_{\rm spu}(x,\ t) = \chi\ [2\ V(x) - V(x\text{-ct}) - V(x + \text{ct})]$, which matches the spurious solutions found numerically. It shows that these solutions are linear in $\rm q_{ext}$, and with regard to more general applications for non-point like distributions in 3D, possibly a wave-like equation $(\partial_{\rm ct}{}^2 - \nabla^2)\ \rho_{\rm spu}(\mathbf{r},\ t) = 8\ \pi\ \chi\ q_{\rm ext}(\mathbf{r})$, could be examined. However, presently any three-dimensional generalizations of the required subtraction-based techniques for the Dirac and FW theories have not been performed neither analytically nor numerically.

3.3 Traditional asymptotic methods

While all of the approaches described above have been developed just within the last decade, for completeness, we review here also very briefly the two more traditional methods, which were historically the first ones that permitted us access to the physics of the vacuum polarization by static charge configurations, such as provide by highly charged nuclei. In the first method (Sect. 3.3.1), the calculation of the density is based on perturbative Feynman diagrams and therefore captures only the lowest order contributions. The second method (Sect. 3.3.2) requires a diagonalization of the Dirac Hamiltonian.

3.3.1 First-order Feynman diagram-based approach

As this approach is detailed in many text books [33], for a direct comparison with our results obtained above, we briefly present here only the final result of its application to our one-dimensional model system [34]. In the perturbative Feynman diagram-based approach, one can compute how the generation of virtual electron–positron pairs give rise to a modification of the Coulomb potential. Using the one-loop vacuum polarization tensor in 1 + 1 space–time dimensions, the charge density can be found (up to first order of the fine structure constant α) analytically as

$$\rho_{\rm Feyn}(x) = q_{\rm ext}\alpha\lambda^{-1}\int_1^\infty {\rm d}\tau\tau^{-3}(\tau^2-1)^{-1/2}\exp\left(-2\tau|x|/\lambda\right) \tag{3}$$

For small distance $|x|$, this complicated (unitless) integral can very well be approximated by $\approx \pi/4$ exp(–2.36 $|x|/\lambda$). For more details and an interesting discussion about the non-trivial role of the fine structure constant in one and three-dimensional systems, see

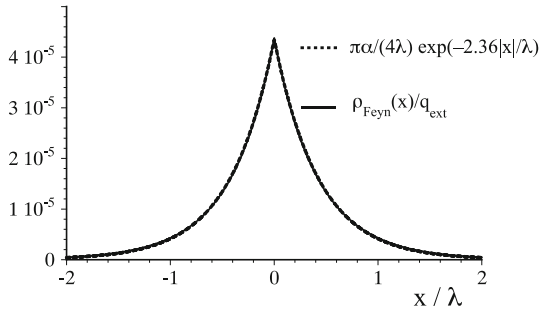

Fig. 6 The lowest-order prediction of the (scaled) charge density based on a Feynman diagram together with the simple functional form $\alpha\pi/(4\lambda)$ exp(− 2.36 $|x|/\lambda$)

[35]. While the integral in Eq. (3) cannot be further simplified, it turns out that induced charge density is very well matched by the simpler numerically fitted density $\rho_{\rm Feyn}(x) \approx q_{\rm ext}\ \alpha\ \lambda^{-1}\ (\pi/4)$ exp(− 2.36 $|x|/\lambda$). In Fig. 6, we illustrate the quality of this approximation.

3.3.2 Diagonalization approach

The derivation for this approach is based again on the interpretation of the process in the Schrödinger picture of this quantum field theoretical process for the case where the external charge $\rm q_{ext}$ is adiabatically slowly turned on. Here, we expect that the system, which is initially in its lowest energetic energy eigenstate, stays in the instantaneous eigenstate of the changing quantum field theoretical Hamiltonian, i.e. the bare vacuum state $|\Phi(\text{t} = 0)\rangle = |\text{vac}\rangle$ evolves adiabatically into the final dressed vacuum state $|\Phi\ (t \to \infty)\rangle = |\text{VAC}\rangle$. Likewise, each of the energy eigenstates for $V_0 = 0$ evolve into the eigenstates of the fully coupled Hamiltonian. It is therefore computationally advantageous, to expand the electron–positron field operator in Eq. (A.2) from the very beginning in terms of the dressed energy eigenstates, defined as $h\ \Phi_{\rm P}(u;x) = E_{\rm P}(u)\ \Phi_{\rm P}(u;x)$ and $h\ \Phi_{\rm P}(d;x) = E_{\rm P}(d)\ \Phi_{\rm P}(d;x)$, where (due to the lack of momentum conservation) the index P is no longer the momentum but a label to characterize the energy of each state. The resulting expansion of the field operator is given by $\Psi(x,t = 0) = \sum_{\rm P}\ B_{\rm P}\ \Phi_{\rm P}(u;x) + \sum_{\rm P}\ D_{\rm P}{}^\dagger\ \Phi_{\rm P}(d;x)$, with the dressed annihilation operators $B_{\rm P}\ |\text{VAC}\rangle = 0$ and $D_{\rm P}\ |\text{VAC}\rangle = 0$. With regard to the asymptotic density, we obtain $\rho(x,\ t \to \infty) = \langle\Phi(t \to \infty)|\ Q(x,\ t = 0)|\ \Phi(t \to \infty)\rangle = \langle\text{VAC}|\ Q(x,\ t = 0)|\text{VAC}\rangle$ which leads to

$$\langle\text{VAC}|\,Q(x,t=0)|\text{VAC}\rangle = e\left[\sum_p|\Phi_P(d;x)|^2 - \sum_p|\Phi_P(u;x)|^2\right]/2 \tag{4}$$

In Fig. 7, we compare this prediction with the densities obtained from all the prior four methods discussed above and it is clear that they agree perfectly within the numerical accuracy of each method. We should

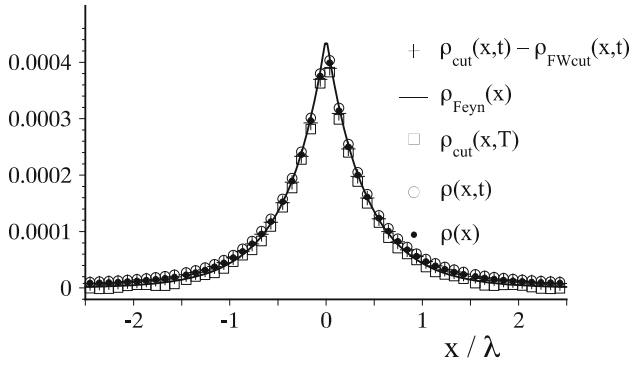

Fig. 7 A comparison of the five steady state vacuum polarization densities $\rho(x,\ t \to \infty)$ obtained by the five methods detailed above for $q_{\rm ext} = 10$.a.u.. The continuous line is from Eq. (3), the crosses are from method 3.2.1 with abrupt turn-on and at time $t = 15\,\tau$ and $E_{\rm cut} = 257.361\ {\rm mc}^2$, the squares are from method 3.2.2 at (periodic) time $T = L/c$ and $E_{\rm cut} = 257.361\ {\rm mc}^2$, the open circles are from method 3.1.2 at time $t = 15\tau$, and the small closed dots are from Eq. (4) according to method 3.3.2 without energy cut-off

note that the electric charge $q_{\rm ext}$ was chosen sufficiently small such that the corrections to the third-order correction to the Feynman density is not so large.

3.3.3 Points of critique and open questions

The diagonalization method requires analytical or computational access to all energy continuum and bound eigenstates. It is known from early pioneering works of Wichmann and Kroll [35], Gyulassy [36], Rinker and Wilets [37] for hydrogenic systems in three spatial dimensions that there are divergent contributions that are linear in the nuclear charge Ze that need to be isolated and removed. The mathematical origin of them is -in our opinion- not really fully understood. The instantaneous elimination technique discussed in Sect. 3.2.1 could also be implemented for the diagonalization-based approach. This has the advantage that one could also include an energy cut-off and therefore not all energy eigenstates need to be calculated. Unfortunately, both the diagonalization, as well as the Feynman method, are steady state approaches, which means that they can predict only final asymptotic charge densities and fail to be applicable for relevant polarization studies of time-varying external electromagnetic fields, that can be now established in the laboratory. Another major drawback of the Feynman based approach is certainly its intrinsic perturbative character as well as the required renormalization procedures to remove unphysical divergencies. It also seems challenging to generalize this approach to external non-point-like charge distributions.

4 Nonlinear corrections to the charge density

In this last section, we illustrate the power of the non-perturbative methods detailed above to examine the higher-order corrections $(q_{\rm ext})^n$ to the vacuum polarization charge density. The motivation to better understand these corrections is three-fold. First of all, we need to comprehend when and how these contributions correct the predictions based on the lowest order, second, they might be relevant to be included in view of experimental available high power laser systems, and third, they also allow for a nice illustration how the linear superposition principle, which is generic to the linear Maxwell equations, becomes invalid.

Let us assume that the asymptotic charge density can be expanded in odd orders of $q_{\rm ext}$ as $\rho(x) = {\rm e}\sum_{n=1}(q_{\rm ext}/e)^{\rm n}\ \rho_n(x)$. The functional form of the (lowest-order) linear spatial distribution $\rho_1(x)$ has been discussed in Sect. 3.2.1 and is well approximated by the form $\rho_1(x) \sim \exp(-\ 2.36\ |x|/\lambda)$ as we showed in Fig. 6. In order to extract numerically the spatial form of the third-order correction $\rho_3(x)$ from the non-perturbative $\rho(x)$, which -in principle- contains all odd orders in ${q_{\rm ext}}^n$, we have first computed two densities $\rho(x)$ and $\rho'(x)$ associated with two different point charges $q_{\rm ext}$ and $q'_{\rm ext}$. We have used here the diagonalization method without energy cut-off (Sect. 3.2.2), which seems to be the most efficient approach for this purpose. In order to eliminate the linear term ρ_1(x) from $\rho(x)$ and to isolate $\rho_3(x)$, we have calculated the difference $[({\rm q_{ext}/e})^2-({\rm q_{ext}'/e})^2]^{-1}[\rho(x)/q_{\rm ext} - \rho'(x)/q'_{\rm ext}]$ which should be equal to $\rho_3(x)$, if we can neglect even higher order terms. For consistency and as a check of the numerical convergence, this procedure was then repeated for several pairs $\{q_{\rm ext},\ q_{\rm ext}'\}$. We found identical distributions ρ_3(x) in the range $2 \times 10^3 < q_{\rm ext} < 4 \times 10^4$. Obviously, if $q_{\rm ext}$ was too large, then higher than cubic corrections play a role while for choices of too small $q_{\rm ext}$ numerical inaccuracies occurred.

In Fig. 8 shows the spatial dependence of the resulting cubic term $\rho_3(x)$ together with the rescaled shape of ρ_1(x) for comparison. We see that the cubic correction $\rho_3(x)$ takes an entirely different shape than $\rho_1(x)$. In fact, $\rho_3(x)$ is comparatively much wider. At the present stage of our understanding, we do not have any intuitive physical picture why this observed spatial widening of $\rho(x)$ due to the higher order contribution $\rho_3(x)$ can be expected.

Finally, having numerical access to $\rho_3(x)$ permits us to illustrate how the traditional linear superposition principle becomes invalid. While according to this principle- the resulting (linear) polarization density induced by two spatially separate charges located at $x = 0$ and $x = a$ is identical to the sum of the individual densities associated with each charge separately, this is no longer true if the cubic contributions are taken into account. We have illustrated this in Fig. 8b and c, where we compared the correct $\rho_3(x)$ that was induced by the

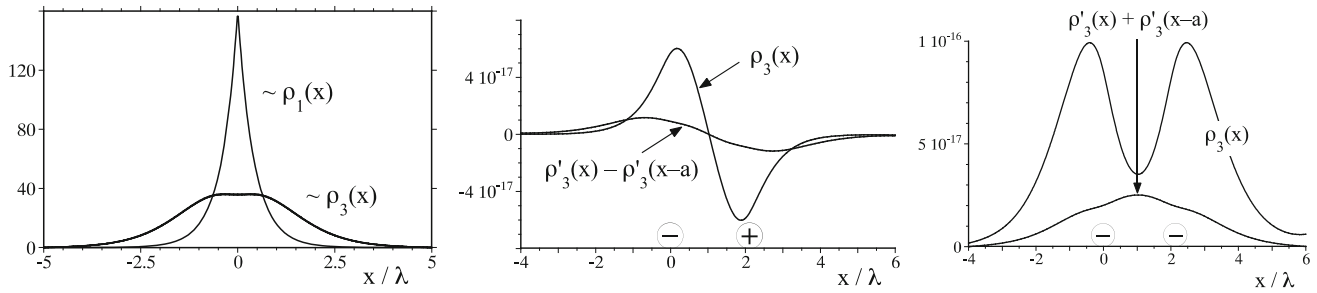

Fig. 8 **a** Comparison of the (scaled) linear and (scaled) cubic contribution to the vacuum polarization charge density induced by a point charge at location $x = 0$. For a better comparison, we have graphed $\rho_1(x)/(2.7 \times 10^{-6})$ and $\rho_3(x)/(4.1 \times 10^{-19})$ such that they have identical areas equal to one. The four matching graphs labeled as $\rho_3(x)$ were obtained for $q_{\text{ext}} = 4000$, 10,000, 20,000, 40,000 a.u. **b** Illustration of the violation of the linear superposition principle for the vacuum polarization density induced by an external dipole. We compare the cubic portion of the density $\rho_3(x)$ induced by a negative external point charge located at $x = 0$ and a positive charge at $x = a = 0.015$ a.u. with the prediction based on linear superposition principle given by $\rho_3'(x) - \rho_3'(x - a)$, where $\rho'_3(x)$ is computed from a single charge at $x = 0$. **c** Same as in Figure b, but the two charges were chosen with equal signs, such that the comparative curve based on the superposition principle is $\rho_3(x) + \rho_3(x - a)$

two external point charges [with density $- q_{\text{ext}}\ \delta(x) + q_{\text{ext}}\ \delta(x - a)$], with the sum $\rho_3'(x) + \rho_3'(x - a)$, where $\rho_3'(x)$ denotes the density induced by a single charge $- q_{\text{ext}}\ \delta(x)$. The disagreement between the true density $\rho_3(x)$ and $\rho_3'(x) - \rho_3'(x - a)$ is obvious. In fact, in the region around $x = 0$ between both charges, the true induced charge density is actually much larger than predicted by the linear superposition principle. The same under-estimation of the correct density (when assuming the superposition principle) is also present if the two inducing charges have the same sign as shown in Fig. 8c. At the present stage of development of experimental laser systems, these predicted non-linear corrections to the vacuum polarization density might be only of academic interest. However, in our view, it nevertheless remains a worthwhile challenge to explore even those predictions of QED that are outside our present technology for their direct detection.

5 Summary and conclusions

In this roadmap to future theoretical studies on QED, we have introduced two new time-dependent computational approaches to study the formation of polarization charges induced by strong external fields from the Dirac vacuum. We also critically examined five different computational approaches to study the vacuum polarization process and argued that in view of the space–time conditions provided by ultra-short intense laser pulses that the traditional static approaches might no longer be sufficient to provide reliable insights into the processes. While this roadmap has focused its attention to the vacuum polarization induced by external fields with subcritical strength, the time-dependent methods are also applicable to more general situations of supercritical fields, which permit the irreversible generation of real electron–positron pairs. Here the occurrence of polarization charges is accompanied by the production of real charges, which makes a space–time resolved analysis significantly more difficult. In this context, we refer the reader to recent proposal [13, 38], where machine learning techniques were employed to examine the particle dynamics inside a supercritical pair creation regime.

Acknowledgements C.G. would like to thank ILP for the nice hospitality during his visit to Illinois State University and acknowledges the China Scholarship Council program. This work has been supported by the NSF and Research Corporation, by the Fundamental Research Funds for the Central Universities (202226943), and by the NSFC under grant No. 11974419. Several computations were performed at the HPC of Illinois State University.

Author contributions

All authors have contributed equally to the paper.

Data Availability Statement This manuscript has no associated data or the data will not be deposited. [Authors' comment: All data generated or analyzed during this study are included in this published article in graphical form.]

Appendix 1

In one spatial dimension, the Dirac Hamiltonian is given by

$$h = c\sigma_1 p + m c^2 \sigma_3 + e V(x,t), \tag{5}$$

where p is the momentum operator and we assume the coupling to a negative charge $- e$. We use from now on

the atomic unit $= \hbar = m = e = 1$ system for our numerical examples. Here the speed of light is $c = 137.036$ a.u. The two 2×2 Pauli-matrices are denoted by σ_1 and σ_3 and V(x,t) is the scalar potential. The generalization of this approach to three spatial dimensions is conceptually straight forward, but requires more extensive resources such as CPU time and memory for its numerical implementation.

As characteristic of any realistic external field, we assume here that $V(x, t)$ vanishes for all negative times. We focus here on the case where the initial quantum state is void of any matter, i.e., $|\Psi(t = 0)\rangle = |\text{vac}\rangle$. The vacuum state permits us to introduce the corresponding set of fermion creation and annihilation operators, denoted by $b(p)^\dagger$, $d(p)^\dagger$, $b(p)$ and $d(p)$. They fulfill the usual fermionic anticommutator relationships, $[b(p),\ b(p')^\dagger]_+ = \delta(p–p')$ and $[b(p),\ b(p')]_+ = 0$. For times $t < 0$, they have an unambiguous interpretation. If they act on the bare vacuum state $|\text{vac}\rangle$, they excite the modes given by the corresponding single-particle states, i.e., $b_p{}^\dagger\ |\text{vac}\rangle = |u;p\rangle$ and $d_p{}^\dagger\ |\text{vac}\rangle = |d;p\rangle$ with momentum p, where the notation u and d denotes states up and down the energy gap between $\pm\ mc^2$.

The electron–positron field operator $\Psi(x,\ t)$ fulfills simultaneously [23] the time-dependent Dirac equation $i\ \hbar\ \partial\Psi/\partial t = h\ \Psi$ or equivalently as well as the Heisenberg equation of motion $i\ \hbar\ \partial\Psi/\partial t = [H,\ \Psi]$, where H is the corresponding quantum field theoretical Hamiltonian given by $H = \int dx\ \Psi(x,\ t)^\dagger\ h\ \Psi(x,\ t)$. Without any loss of generality, one can choose an arbitrary set of basis states for the expansion of this operator $\Psi(x,\ t)$ as

$$\psi(x,t) = \Sigma_p b_p(t)\phi_p(u;x)\ + \Sigma_p d_p^\dagger(t)\phi_p(d;x) \tag{6}$$

$$\psi(x,t) = \Sigma_p b_p\phi_p(u;x,t)\ + \Sigma_p d_p^\dagger\phi_p(d;x,t) \tag{7}$$

Traditionally, one often chooses the positive and negative energy eigenstates in this "mode-expansion", where p labels their momentum. These energy eigenstates fulfill $h_0|u;\ p\rangle = e_p|u;\ p\rangle$ and $h_0|d;\ p\rangle = -\ e_p|d;\ p\rangle$ with $e_p \equiv [m^2c^4\ +\ c^2p^2]^{1/2}$ and have the spatial representation $\langle x|u;\ p\rangle \equiv \phi_p(u;\ x)$. The force-free Dirac Hamiltonian is given by $h_0 \equiv c\ \sigma_1\ p\ +\ \sigma_3\ mc^2$. The lower (label d) and upper (label u) energy eigenstates $|p;\ d\rangle$ and $|p;\ u\rangle$ are known analytically and take the spatial representation by the two-component spinors, $\phi_p(u,\ x,\ t) = \langle x|p;\ u\rangle = N\ \{[e_p\ +\ mc^2]^{1/2},\ [e_p–mc^2]^{1/2}\ p/|p|\}\ \exp[ipx/\hbar]$ and $\phi_p(d,\ x,\ t) = \langle x|p;\ d\rangle = N\ \{–[e_p\ –\ mc^2]^{1/2}\ p/|p|,\ [e_p\ +\ mc^2]^{1/2}\}\ \exp[ipx/\hbar]$, where N is the corresponding normalization factors.

If we equate Eqs. (6) and (7) and use the orthogonality between the basis states, we can express the time-evolved creation and annihilation operators in terms of the initial ones (at $t = 0$) as

$$b_p(t) = \Sigma_{p'} b_{p'}\langle u;p\ |u(t);p'\rangle + \Sigma_{p'} d_{p'}^\dagger\langle u;p\ |d(t);p'\rangle \tag{8}$$

$$d_p^\dagger(t) = \Sigma_{p'} b_{p'}\langle d;p|u(t);p'\rangle + \Sigma_{p'} d_{p'}^\dagger\langle d;p|d(t);p'\rangle \tag{9}$$

The set of four transition matrix elements $\langle u;p\ |u(t);p'\rangle$, $\langle u;p\ |d(t);p'\rangle$, $\langle d;p\ |u(t);p'\rangle$ and $\langle d;p\ |d(t);p'\rangle$ are the fundamental building blocks of computational quantum field theory. The time-evolution of the creation and annihilation operators given by Eqs. (A.3) is valid for any sub- or supercritical dynamics. Once this set is known, any other desired observable, such as spatial, momentum or energy densities and the created pair numbers with the time evolution, can be calculated from it. In order to determine these matrix elements, every single state of the Hilbert space $|u;p\rangle$ and $|d;p\rangle$ has to be evolved in time, and then the corresponding projections can be calculated.

The fully coupled electron–positron field operator $\Psi(x,t)$ itself can be uniquely defined and calculated independently of the basis representation even for the interesting supercritical field regime where the number of particles can change in time. As a result, also the total charge density can always be obtained from the corresponding expectation values of the charge density operator, given by $Q = -\ e\ (\Psi^\dagger\Psi\ –\ \Psi\Psi^\dagger)/2$. If we insert the above expansions for Ψ into Q and compute the expectation value with regard to $|\text{vac}\rangle$, we obtain

$$\rho(x,t) \equiv (e/2)\Sigma_p[|\phi_p(d,x,t)|^2 – |\phi_p(u,x,t)|^2] \tag{10}$$

where the summation for $\phi_p(d,\ x,\ t)$ and $\phi_p(u,\ x,\ t)$ extends over all states with an initially negative and positive energy, respectively.

References

1. For a very recent and extensive review, see, e.g., Advances in QED with intense background fields, A. Fedotov, A. Ilderton, F. Karbstein, B. King, D. Seipt, H. Taya and G. Torgrimsson. arXiv:2203.00019 [hep-ph] (2022)
2. B.S. Xie, Z.L. Li, S. Tang, Electron-positron pair production in ultrastrong laser fields. Matter Radiat. Extrem. **2**, 225 (2017)
3. A. Di Piazza, C. Müller, K.Z. Hatsagortsyan, C.H. Keitel, Extremely high-intensity laser interaction with fundamental quantum systems. Rev. Mod. Phys. **84**, 117 (2012)
4. P.M.A. Dirac, Discussion of the infinite distribution of electrons in the theory of the positron. Camb. Phil. Soc. **30**, 150 (1934)
5. W. Heisenberg, Bemerkungen zur Diracschen Theorie des Positrons. Z. Phys. **90**, 209 (1934)
6. R. Serber, Linear modifications in the Maxwell field equations. Phys. Rev. **48**, 49 (1935)
7. E.A. Uehling, Polarization effects in the positron theory. Phys. Rev. **48**, 55 (1935)

8. A.T. Steinacher, J. Betke, S. Ahrens, Q. Su, R. Grobe, Space-time dynamics of the vacuum's polarization charge density. Phys. Rev. A **89**, 062106 (2014)
9. Q.Z. Lv, J. Betke, Q. Su, R. Grobe, A time-dependent charge renormalization procedure in QED. Phys. Rev. A **92**, 032121 (2015)
10. See, for example, M. Marklund, T.G. Blackburn, A. Gonoskov, J. Magnusson, S.S. Bulanov and A. Ilderton, Towards critical and supercritical electromagnetic fields. arXiv:2209.11720 (2022)
11. See, for example, the executive summary of the workshop "Brightest Light Initiative" held March 2019 in Washington, DC, A Community Plan for Fusion Energy and Discovery Plasma Sciences, by S. Baalrud, N. Ferraro, L. Garrison, N. Howard, C. Kuranz, J. Sarff, W. Solomon. arXiv:2011.04806 (2020)
12. See, for example, APS-DPP Community Planning Process, and the recent report by the National Academy of Sciences, Engineering and Medicine, entitled "A Decadal Assessment of Plasma Science" (2020)
13. C. Gong, J. Bryan, Q. Su, R. Grobe, Machine learning techniques in the examination of the electron-positron pair creation process. J. Opt. Soc. Am B **38**, 3582 (2021)
14. C. Gong, Q. Su, R. Grobe, Vacuum polarization is not a precursor for permanent pair creation. J. Phys. B **54**, 135601 (2021)
15. P.W. Miloni, *The Quantum Vacuum* (Academic Press, 1993)
16. R.W. Boyd, *Nonlinear Optics*, 4th edn. (Elsevier, Academic Press, London, 2020)
17. Q. Su, J.H. Eberly, J. Javanainen, Dynamics of atomic ionization suppression and electron localization in an intense high-frequency radiation field. Phys. Rev. Lett. **64**, 862 (1990)
18. Q. Su, J.H. Eberly, Model atom for multiphoton physics. Phys. Rev. A **44**, 5997 (1991)
19. A.D. Alhaidari, Relativistic Coulomb problem for Z larger than 137. https://arxiv.org/ftp/arxiv/papers/1005/1005.1414.pdf (2010)
20. M. Ruf, C. Müller, R. Grobe, Numerical signatures of non-self adjointness in quantum Hamiltonians. J. Phys. A **44**, 345205 (2011)
21. J. Rafelski, J. Kirsch, B. Müller, J. Reinhardt, W. Greiner, Probing QED vacuum with heavy ions. http://arxiv.org/pdf/1604.08690.pdf (2016)
22. I. Bialynicki-Birula, Z. Bialynicka-Birula, *Quantum Electrodynamics* (Pergamon, Oxford, 1975)
23. W. Greiner, B. Müller, J. Rafelski, *Quantum Electrodynamics of Strong Fields* (Springer Verlag, Berlin, 1985)
24. T. Cheng, Q. Su, R. Grobe, Introductory review on quantum field theory with space-time resolution. Cont. Phys. **51**, 315 (2010)
25. J.A. Fleck, J.R. Morris, M.D. Feit, Time-dependent propagation of high energy laser beams through the atmosphere. Appl. Phys. **10**, 129 (1976)
26. A.D. Bandrauk, H. Shen, High-order split-step exponential methods for solving coupled nonlinear Schrodinger equations. J. Phys. A **27**, 7147 (1994)
27. J.W. Braun, Q. Su, R. Grobe, Numerical approach to solve the time-dependent Dirac equation. Phys. Rev. A **59**, 604 (1999)
28. G.R. Mocken, C.H. Keitel, FFT-split-operator code for solving the Dirac equation in 2+1 dimensions. Comp. Phys. Commun. **178**, 868 (2008)
29. P. Krekora, Q. Su, R. Grobe, Relativistic electron localization and the lack of Zitterbewegung. Phys. Rev. Lett. **93**, 043004 (2004)
30. R.E. Wagner, B.T. Shields, M.R. Ware, Q. Su, R. Grobe, Causality and relativistic localization in one-dimensional Hamiltonians. Phys. Rev. A **83**, 0621106 (2011)
31. R.E. Wagner, M.R. Ware, E.V. Stefanovich, Q. Su, R. Grobe, Local and non-local spatial densities in quantum field theory. Phys. Rev. A **85**, 022121 (2012)
32. L.L. Foldy, S.A. Wouthuysen, On the Dirac theory of spin $\frac{1}{2}$ particles and its non-relativistic limit. Phys. Rev. **78**, 29 (1950)
33. M.D. Schwartz, *Quantum Field Theory and the Standard Model* (Cambridge University Press, Cambridge, 2013)
34. Q.Z. Lv, N.D. Christensen, Q. Su, R. Grobe, Validity of one-dimensional QED for a system with spatial symmetry. Phys. Rev. A **92**, 052115 (2015)
35. E.H. Wichmann, N.M. Kroll, Vacuum polarization in a strong Coulomb field. Phys. Rev **101**, 843 (1956)
36. M. Gyulassy, Higher order vacuum polarization for finite radius nuclei. Nucl. Phys. A **244**, 497 (1975)
37. G.A. Rinker, L. Wilets, Vacuum polarization in strong, realistic electric fields. Phys. Rev. A **12**, 748 (1975)
38. C. Gong, Q. Su, R. Grobe, Birth process of elementary particles inside supercritical fields. Phys. Rev. Lett. (under review)